This is a Preprint and has not been peer reviewed.

Title

Statistical properties and modelled duration of an intracontinental earthquake sequence: 2021 Mw 5.9 Woods Point earthquake, Australia

Authors

Yunqi Huang[1], Mark Quigley[1,2], James La Greca[1,2], Jake Wilcox[2], Elodie Borleis[2], Eleanor Green[1], Wayne Peck[2]

Affliations

1. School of Geography, Earth, and Atmospheric Science, The University of Melbourne, Parkville, Australia

2. Seismology Research Center, 141 Palmer Street, Richmond VIC 3121 Australia

Corresponding Email Address: yunqhuang@student.unimelb.edu.au

Abstract

We investigate the 2021 moment magnitude (M_w) 5.9 Woods Point earthquake aftershock sequence (WPAS) in Victoria, Australia. WPAS Gutenberg-Richter b-values range from 0.76 to 1.07 and depend upon the earthquake magnitude type used (Mw vs Ml) and minimum completeness magnitude (Mc). The WPAS Modified Omori's law *p*-value of 0.83~0.84 suggests slower aftershock decay rates, while the modelled duration of the WPAS (7.5 to 40.4 years) is consistent with estimated aftershock sequence durations in comparable continental intraplate settings. The high double-couple (>80%) of the mainshock and strong statistical fit of a sub-vertical plane to the aftershock cloud favour a structurally simple mainshock source fault. However, the delayed occurrence of the largest aftershocks (Ml 4.7, 4.2) and high proportion (~70%) of WPAS moment release sourced at distances > 1.5 km from the mainshock fault suggests aftershock activity on nearby structurally complex fault networks, as observed in other Australian sequences.

Keywords: Woods Point Earthquake, Intraplate Earthquake, Statistical Seismology

1 Introduction

Aftershock sequences may be protracted in time and space and present numerous hazards to people, infrastructure, and landscapes (e.g., Quigley et al., 2016). In a typical earthquake sequence, the mainshock is associated with the largest seismic moment release (Shcherbakov & Turcotte, 2004) and the subsequent aftershocks (i.e., smaller-magnitude earthquakes in the time-and-space vicinity of the mainshock) may be triggered by a variety of static, dynamic, and post-seismic stress transfer mechanisms (Freed, 2005). The duration and behaviour of aftershock sequences have been linked to mainshock fault properties, crustal structure, tectonic setting (Stein & Liu, 2009), and other seismotectonic aspects (e.g., Ozawa & Ando, 2021). Stable continental regions (SCRs), where tectonic slip loading occurs more slowly compared to interplate regions (Li et al., 2009; Stein & Liu, 2009), have been proposed to host long-duration (e.g., 10^2-10^3 years) aftershock sequences (Stein & Liu, 2009). Compared to active plate boundaries, the heterogeneous nature of the continental crust, including varying stress responses between the viscous lower crust, upper mantle, and less viscous upper crust (Hearn et al., 2002), combined with complex, interacting fault systems (Liu & Stein, 2016), complicates the prediction of stress transmission and aftershock sequences.

Distinguishing aftershocks from background seismicity becomes increasingly challenging as aftershock rates decay with time. Aftershock duration estimates (i.e., the time it takes for seismicity to decay to background rates) and other seismic parameters (see methods below) are relevant for probabilistic seismic hazard assessments (Toda & Stein, 2018) and operational earthquake forecasts (Jordan et al., 2011).

The 2021 Mw 5.9 Woods Point earthquake in Victoria Australia, stimulated an aftershock sequence (WPAS) including several local magnitude (Ml) ≥ 4 earthquakes (Figure 1) (Ninis et al., 2021). To enhance our understanding of SCR aftershock sequences, we calculate the parameters of the Gutenberg-Richter Law and Modified Omori's Law, model the duration of WPAS, and compare the seismicity spatial distribution and monthly energy release with the pre-mainshock background seismicity. Additionally, we model several rupture planes based on the spatial distribution of the WPAS to assess the distribution of on-fault and off-fault aftershocks.

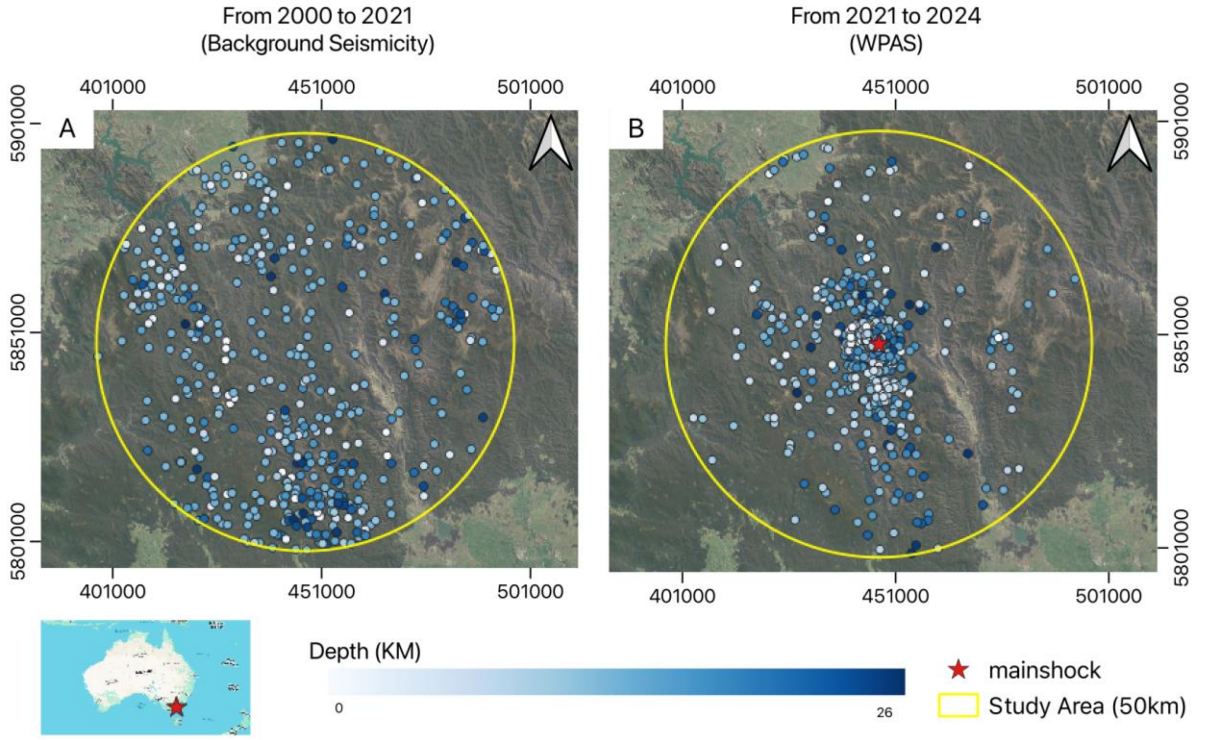

Figure 1. Location of seismicity observed in the Woods Point region. Figure A displays the background seismicity recorded during the pre-mainshock stage (2000 to 2021) within a 50 km radius from the mainshock epicentre (-37.506°, 146.402°). Figure B shows the Woods Point Aftershock Sequence (WPAS) from 2021 to 2024 within the same spatial domain. The depths of the observed events are provided in kilometres below sea level (BSL). The surface elevation in the study area ranges from 350 to 1400 metres. Figures A and B use the EPSG:7855 projected coordinate system. Legend shows the location of the Woods Point Mw 5.9 mainshock.

2 Methodology

The following methods are used in this research:

(i) Magnitude Completeness (Mc) Estimation: We used the Maximum Curvature (MAXC) method (Wyss et al., 1999; Wiemer & Wyss, 2000), the Mc Estimation Based on b-value Stability (MBS) method (Cao & Gao, 2002), and the bootstrapping method (Efron & Tibshirani, 1994) to calculate Mc for background seismicity and WPAS. **(ii) Gutenberg-Richter Analysis:** The Maximum Likelihood Estimation (MLE) method (Aki, 1965; Utsu, 1965) was used for b-value estimation, and the method by Shi & Bolt (1982) was employed for calculating b-value uncertainty. **(iii) Modified Omori's Law**: Parameters were estimated using the MLE method (Ogata, 1983) and Bayesian Analysis (Holschneider et al., 2012). **(iv) Fault Plane Fitting:** We applied the Linear Algebra and Coordinate Rotation methods for fault plane fitting. **(v) Aftershock Modelled Duration**: we used the Seismicity Rate and Energy Monthly Released methods to estimate. Full methodological details are available at GitHub: *https://github.com/Yunqi12/Data-Description-Methodology*

3 Results and Discussion

3.1 Gutenberg-Richter Law

We calculated the a-value and b-value using three different methods to determine the Mc for the pre-WP mainshock background seismicity and the WPAS (Table 1). The MAXC method often underestimates Mc (Wiemer & Wyss, 2000; Mignan & Woessner, 2012), while the MBS method, though more reliable for Mc selection, tends to overestimate it (Woessner & Wiemer, 2005; Mignan & Woessner, 2012). Both methods introduce sampling error due to limited time and space windows (Table 1). To mitigate this, we combined the bootstrapping method with both Mc estimation methods. The Mc values estimated by the MAXC and MBS methods fall within the uncertainty range of the MAXC+bootstrapping and MBS+bootstrapping methods respectively. However, there is a trade-off between using smaller Mc values (i.e., incorporating more earthquakes but reducing confidence in catalogue completeness) and larger Mc values (i.e., including fewer earthquakes, which reduces the sample size for statistical data fitting but improves confidence that all events above Mc are recorded, as shown in Figure 2). Thus, our preferred Mc is an intermediate value between MAXC + Bootstrapping and MBS + Bootstrapping, as it balances maintaining sample size, and ensuring reliable event observation.

Table 1. Summary of results from the Woods Point regional seismicity study, organised by time period and magnitude format, based on frequency-magnitude distribution. Note: The MAXC method for Mc estimation, along with bootstrap resampling, and the MLE method for b-value calculation, including b-value uncertainty, were implemented using code adapted from the 'Basic Statistical Seismology Tutorial' by Sullivan & Peng (2011). [http://geophysics.eas.gatech.edu/people/bsullivan/tutorial/StatisticalSeismology.htm].

		Time Period					
		Background Seismicity (2000 to 2021)		Synthetic Background Seismicity (Leonard, 2008)**	Regional Background Seismicity (Allen et al., 2018)***	WPAS (2021 to 2024)	
		Ml	Mw	Ml	Mw	Ml	Mw
Mc (*n)**	MAXC	1 (*327*)	1.8 *(327)*			0.6 *(1349)*	1.5 *(1349)*
	MAXC+ Bootstrapping	0.90+/-0.24 *(272~416)*	1.71+/-0.18 *(272~384)*			0.61+/-0.06 *(1186~1349)*	1.50+/-0.02 *(1046~1349)*
	MBS	3.3 *(26)*	2.9 (*79*)	2.0~2.5	2.85	0.9 *(923)*	1.9 *(556)*
	MBS+ Bootstrapping	3.16+/-0.22 *(22~38)*	2.89+/-0.18 *(48~88)*			1.00+/-0.13 *(556~923)*	1.85+/-0.08 *(456~800)*
	Preferred Mc	2.03+/-0.23 *(93~170)*	2.3+/-0.18 *(131~197)*			0.80+/-0.1 *(923~1046)*	1.68+/-0.06 *(800~923)*
GR Law	Observed Catalogue	b=0.58+/-0.04,a=3.29	b=0.73+/-0.04,a=3.94	b=0.9, a=2.93	b = 1.08	b=0.76+/-0.02,a=3.63	b=1.07+/-0.03,a=4.79

* *Number of earthquakes in the analysed catalogue greater or equal to Mc*

*** Leonard (2008) suggested a Mc value for Southeast Australia since 1995, identifying the magnitude threshold based on the linear relationship of the frequency-magnitude distribution. Regarding the a-value of the Gutenberg-Richter Law, Leonard's result indicates a value of 3.7 per century per 10,000 km² for Southeast Australia. As the a-value reflects regional seismicity and is influenced by both the time window and spatial domain, the smoothed a-value from Leonard's result, adjusted for our study domain, is approximately 2.93.*

**** Allen et al. (2018) suggested a magnitude of completeness (Mc) of Mw 2.85 for Southeast Australia since 1966, estimated based on the National Catalogue Completeness Models. The b-value for the Otway-Sorell-Gippsland Basin zone in Southeast Australia was calculated using the National Seismic Hazard Assessment Earthquake Epicentre Catalogue (NSHA18-Cat).*

Table 1 also compares b-values calculated from the WPAS with several other regional estimates. As discussed by e.g. Nava et al. (2017), a smaller sample size (i.e. higher Mc) reduces the number of events available for b-value estimation, thereby affecting the fitting accuracy. Figure 2 shows the relationship between the b-value estimate and its uncertainty as a function of the chosen Mc, as calculated for the various methods in this study. The b-value is also significantly affected by the magnitude type, due to the non-linear conversion between Ml and Mw (for the conversion equation, see Appendix 1 - Data Description, Equation S1: *https://github.com/Yunqi12/Data-Description-Methodology*). Regardless of the preferred Mc and magnitude type, however, the WPAS b-values lie on the high side of the uncertainty range of b-values estimated from pre-mainshock background seismicity.

When comparing our results with other Australian studies of the GR Law, we find that the pre-mainshock background seismicity b-value for Ml is lower than the value (i.e., 0.9) calculated for Southeast Australia by Leonard (2008), and the pre-mainshock background seismicity b-value for Mw is lower than the value of 1.078 suggested by Allen et al. (2018) for regional background seismicity; however, our b-values from the WPAS (ranging from 0.76 to 1.07) are consistent with both Leonard (2008) and Allen et al. (2018). The discrepancy between our b-value for background seismicity and those from Leonard (2008) and Allen et al. (2018) is likely due to the limited spatial and temporal extent of our background seismicity model (2000 to 2021), which results in a relatively small dataset (93 to 197 events). However, the b-value obtained for the offshore Gippsland Basin, Southeast Australia by Attanayake et al. (2023) between 2009 and 2021 ranges from 0.6 to 0.73 (using an Mc cutoff between Ml 0.7 and Ml 1.2) based on the MLE method, which is similar to our b-value for Ml background seismicity (0.58 ± 0.04), despite Attanayake et al. (2023) using a larger sample size (1145 to 4004 events) to estimate the b-value. Our b-value, similar to that of Attanayake et al. (2023), is more susceptible to sampling bias (e.g., limited temporal and spatial extent) and overfitting (Godano et al., 2014) compared to the b-value estimates from Leonard (2008) and Allen et al. (2018). This is due to epistemic uncertainty in the b-value estimation, leading to two possibilities. Firstly, the low Mc chosen may influence the statistical fitting, potentially causing the MLE method to overfit small-magnitude seismicity, placing less emphasis on larger magnitude events. This results in a lower b-value and an overestimation of predicted seismicity for large magnitudes. Secondly, shifting Mc to a higher magnitude reduces the sample size and increases the weight of large-magnitude events in the fitting. This raises the b-value and increases statistical fitting uncertainty, potentially leading to an overestimation of predicted seismicity for smaller-magnitude events.

Since Leonard's results are based on a catalogue covering the entire Southeast Australia over a century, they may be less susceptible to sampling bias than ours. To align with our study, we adjusted Leonard's research's spatial and temporal extent to our study domain (see Table 1 for results). We then compared the calculated pre-mainshock background seismicity GR Law parameters from this study and Leonard (2008) with the observed earthquake productivity in the Woods Point region. We found that Leonard's b-value (0.9) and smoothed seismicity a-value (2.93) yields lower seismicity rate than the observed seismicity (Figure 3A). In contrast, the b-value (0.58) and a-value (3.29) calculated in this study suggest a higher potential productivity of small-magnitude events (below the Mc cutoff) than what has been observed. There is epistemic uncertainty regarding whether locally observed background seismicity (i.e., the GR Law parameters calculated in this study) or smoothed regional seismicity (i.e., Leonard, 2008) more accurately represents the background seismicity rate for the Woods Point region. The b-value of the Woods Point region is sensitive to Mc selection, catalogue variations, and spatial-temporal variability (Godano et al., 2014). Additionally, the observed seismicity is affected by epistemic and sampling errors, which may induce uncertainty in b-value calculation and Mc selection. Therefore, we calculate the preferred GR relationship parameters for the Woods Point region (Table 1). This was determined by averaging the frequency–magnitude relationship for Leonard's results with our study.

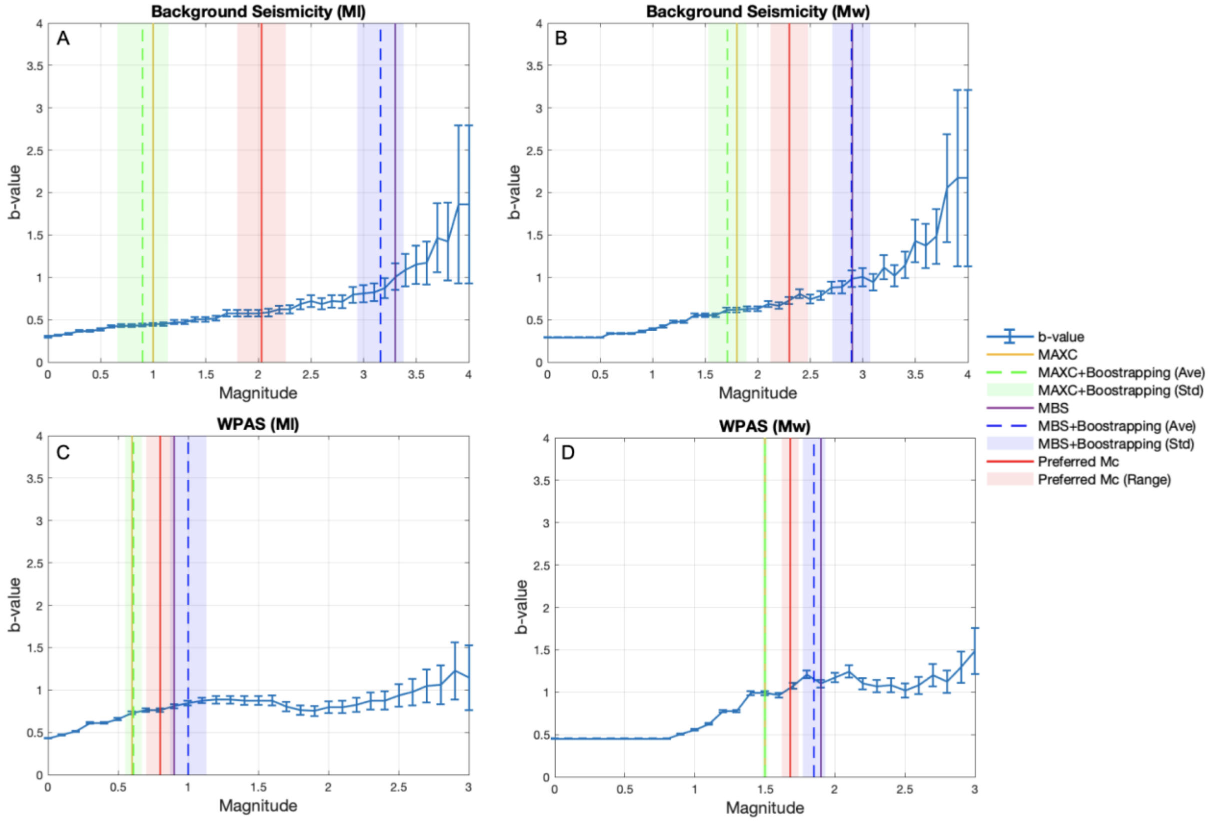

Figure 2. The b-value and its uncertainty vary with the selection of the Mc value. Figure A shows the variability of b-values with different Mc selections for pre-mainshock background seismicity in the Ml catalogue. Figure B shows the results for pre-mainshock background seismicity in the Mw catalogue. Figure C presents the results for the WPAS Ml catalogue, and Figure D presents the results for the WPAS Mw catalogue.

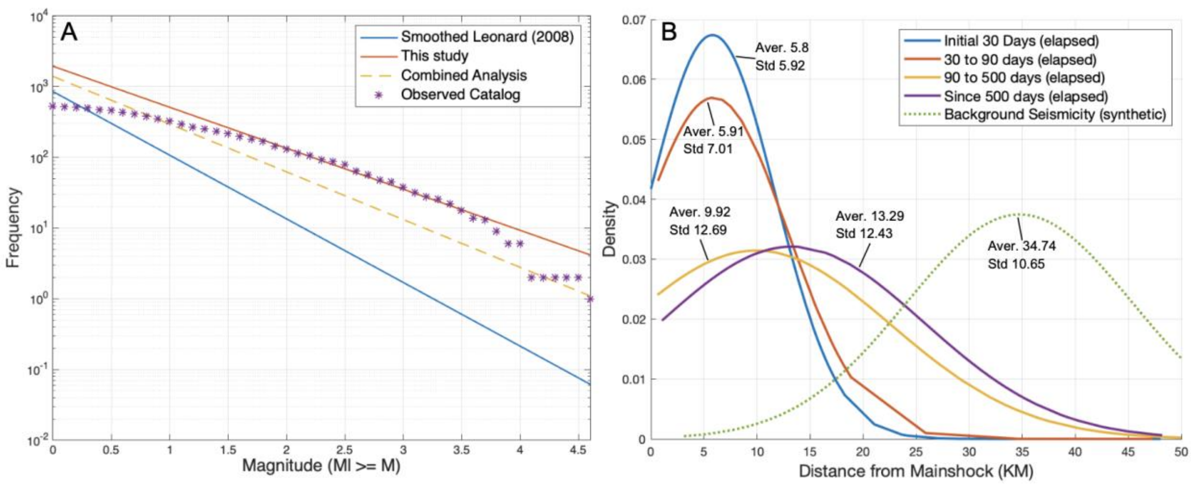

Figure 3. A) Frequency-Magnitude Distribution, including Leonard (2008) smoothed results, this study's model based on observed pre-mainshock background seismicity, and the combined result from Leonard's and the observed pre-mainshock background seismicity. B) Distance Probability Distribution Function (pdf) from the mainshock to the events observed in the Woods Point region across different periods: (1) the first 30 days following the mainshock, (2) from 30 to 90 days following the mainshock, (3) from 90 to 500 days following the mainshock, (4) from 500 days after the mainshock until 7th August 2024, and (5) the synthetic background seismicity prior to the mainshock.

3.2 Modified Omori's Law

Modified Omori's Law was calculated based on the preferred Mc for WPAS (Mc = 0.8 for Ml, and Mc = 1.68 for Mw) (Table 2). The c-value for both magnitude types (Ml and Mw) is 0, indicating that the aftershock sequence follows a power-law decay immediately after the mainshock. However, this parameter is sensitive to the selection of Mc, typically decreasing as Mc increases (Shcherbakov et al., 2012). The k-value, which reflects aftershock productivity and is scaled according to the mainshock's magnitude (Helmstetter & Sornette, 2003), differs between the Ml and Mw catalogues (64.81 or 64.84 for Ml and 56.25 for Mw), primarily due to variations in Mc. The p-value for WPAS for both Ml and Mw is 0.84 and 0.83, respectively. The global average p-value for aftershock sequences is around 1.1 (Utsu et al., 1995). Our p-value, which is less than 1, suggests a relatively slow decay rate of aftershock sequences compared to the global average, including a slower decay than some other sequences in Australia, such as Tennant Creek (1988, Ml 6.8, p = 0.96) (Ebel et al., 2000) and Meckering (1968, Mw 6.6, p = 1) (Ebel, 2009).

Table 2. Some results obtained from the Woods Point Aftershock Sequence (WPAS). Note: The Ogata method and Bayesian method for Modified Omori's Law calculation were implemented using code adapted from "Seishimi" by Liu (2022) [https://github.com/yuankailiu/Seishimi].

		Ml		**Mw**	
		MLE Method	Bayesian Method	MLE Method	Bayesian Method
		c=0, k=64.81, p=0.84	c=0, k=64.84, p=0.84	c=0, k=56.25, p=0.83	c=0, k=56.25, p=0.83
Aftershock Anticipated Duration (days)	Smoothed Leonard (2008)	14759.2	14767.3	-	-
	Model based on Observed Background Seismicity (This study)	2722	2723.5	3590.5	3590.5
	Combined Result	4958.2	4960.9	-	-

3.3 Modelled Duration of the WPAS

As of 7th August 2024 (UTC+0), the current seismicity rate in the Woods Point region (catalogue above Mc cutoff) is above the synthetic pre-mainshock background rate based on the observed catalogue (Figure 4A and B). Based on the modelled background seismicity in this study, the aftershock sequence could end approximately 2722 or 2723.5 days (7.5 years) after the mainshock. Based on the preferred GR Law for background seismicity, with implied lower seismicity rate, the sequence may last around 4958.2 or 4960.9 days (13.6 years). If aligned with Leonard's (2008) smoothed result alone, the aftershock sequence could extend up to 40.4 years. The observation that a Ml 4.2 aftershock on 6th August 2024 suggests that the sequence is still ongoing.

The spatial distribution of all seismicity in the Woods Point region is still clustering near the Woods Point mainshock hypocentre (averaging within 13.29 km) and is distinct from a calculated synthetic background seismicity distribution (Figure 4B). The observed monthly energy release from seismicity in the Woods Point region is still higher than the 68% confidence interval of the monthly energy release observed during the pre-mainshock background seismicity period (Figure 4C and D).

Interplate aftershock sequences typically last less than a decade, with large events ending a few years after the mainshock (Parsons, 2002). In contrast, intraplate earthquakes can extend for hundreds of years (Stein & Liu, 2009), with their aftershock sequences potentially lasting longer due to slow stress loading rates (Li et al., 2009; Stein & Liu, 2009) and heterogeneous crustal structure (Hearn et al., 2002). Our estimated duration (7.5 to 40.4 years) is consistent with the hypothesis of long-duration aftershock sequences in the continent's interior.

3.4 Distribution of moment release in the WPAS relative to the rupture plane

The rupture plane fitted from the aftershock sequence in this study shows similar results to the two published sources of the rupture plane (Table 3). The high double couple of the mainshock (>80% - Mousavi et al., 2023) and good statistical fit of a sub-vertical plance to the WPAS data, suggests a simple mainshock source fault. However, the complex behaviour of aftershock sequences in SCRs introduces additional challenges. For instance, interactions within a complex fault system (Liu & Stein, 2016) may cause deviations from the expected geometric distribution of the rupture plane. These deviations can complicate efforts to statistically fit aftershocks to the rupture plane model, making interpretation and accuracy more difficult.

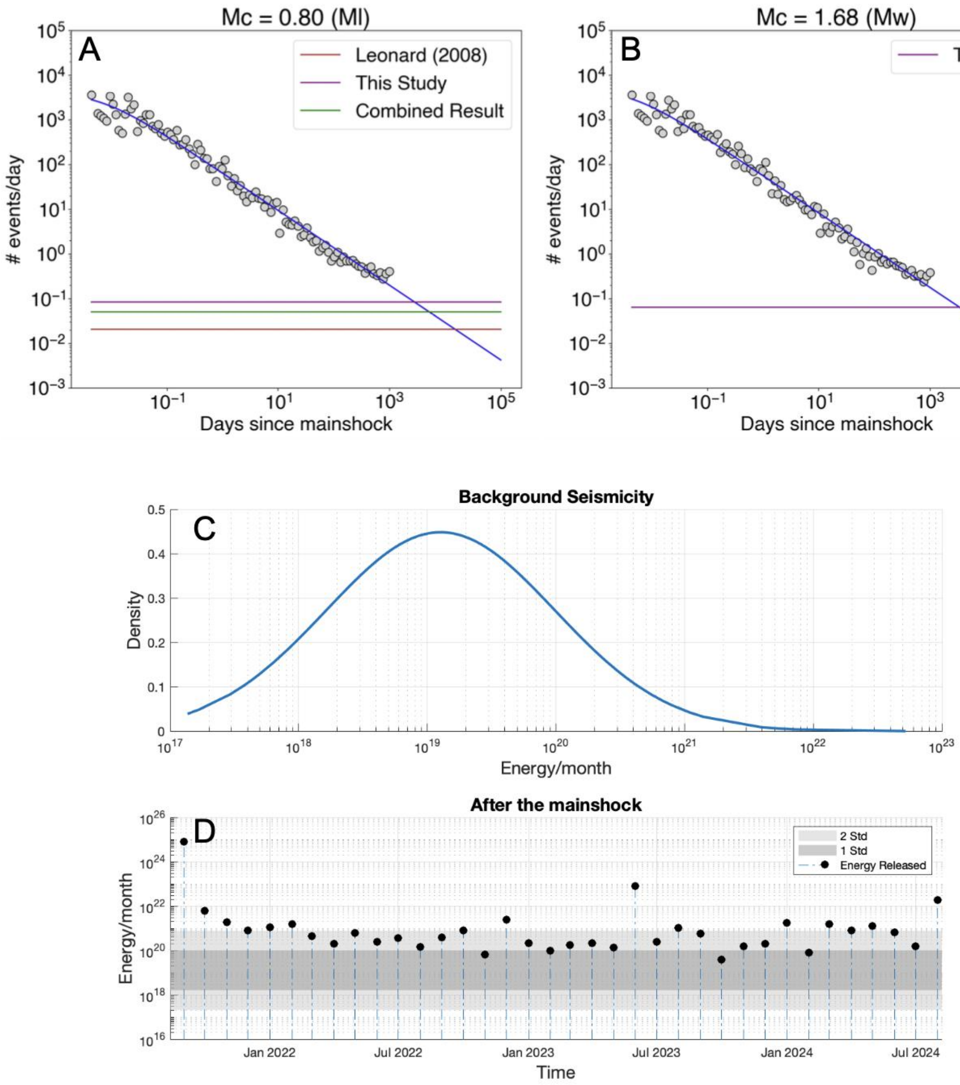

*Figure 4. Comparison of post-mainshock seismicity level with pre-mainshock seismicity level. Figures A and B compare the current seismicity rate with the synthetic background seismicity. Figures C and D show the energy released in the Woods Point region per month (within a 50 km radius from the mainshock hypocenter). Figure C displays the normal distribution of energy released during the pre-mainshock period, while Figure D illustrates the monthly energy release since the mainshock, compared to the pre-mainshock level. The shaded area representing one standard deviation from the pre-mainshock energy distribution includes 68% of the background seismicity, and the area representing two standard deviations includes 95% of the pre-mainshock level. Note**:** Figures A and B were obtained using code adapted from "Seishimi" by Liu (2022) [https://github.com/yuankailiu/Seishimi].*

Table 3. The table below summarises fault planes reported by various researchers, alongside the results obtained from this study.

Source	**Fault Plane**						
	Strike (°)	**Dip (°)**	**Length (Km)**	**Width (Km)**	**Min. Depth (Km)**	**Max. Depth (Km)**	**Aver. Slip (m)**
Mousavi et al. (2023)	348 ± 2	87	-	~8*	11	19	-
Quigley et al. (2021)	350	85	8	9	(ca.) 4	(ca.) 13	-
Preferred Fault Plane (This study)	352.81 +/- 3.2	85.50E +/- 2.97	4.8 ~ 6.6 (aver. 5.96)	6.77 ~ 9.31 (aver. 7.55)	7.63 ~ 8.96 (aver. 8.36)	14.83 ~ 17.82 (aver. 15.88)	0.59

** A rough calculation based on the depth range of the rupture plane and the dip angle provided by Mousavi et al. (2023)*

When we then compare cumulative moment release with distance from all the fault planes fitted to WPAS in this study, we find that the maximum curvature of the moment release is within 1.5km of the fault planes. We define this area as the on-fault aftershock zone, where the amount of energy released accumulates rapidly due to the clustering of aftershocks caused by intense displacement and slip near the rupture plane (Yukutake & Iio, 2017). When considering distance greater than 1.5 km from the fault planes, the energy release rate decays until it reaches 100%. This is with the exception of the Ml 4.2 aftershock in September 2021 (approximately 18 minutes of the mainshock) and the Ml 4.7 aftershock in June 2023 which are interpreted to be off-fault aftershocks. The Ml 4.2 earthquake (which occurred on the 6th of August 2024) is interpreted to be an on-fault aftershock (Figure 5). By 7th August 2024, the on-fault aftershock zone accounted for 29.4% of the total energy released from the WPAS seismicity (i.e., 10km from the rupture plane on each side).

Estimates of earthquake damage zone widths range from 200 to 250m, as observed in the 1992 Mw 7.3 Landers earthquake (Peng et al., 2003), the 2010 Mw 7.1 Darfield earthquake (Li et al., 2014), and the Parkfield segment of the San Andreas Fault (Lockner et al., 2011). Our inferred 1.5 km half-width of the Woods Point mainshock fault zone, determined from the maximum curvature of moment release (Figure 5), is consistent with half-width estimates of seismicity fall-offs from strike-slip earthquakes on slow-slip rate faults in California (e.g., 0.8 to 1 km; Perrin et al., 2021). Considering potential complicating factors, such as epistemic uncertainties in aftershock locations, we estimate the total width of the dilatant damage zone associated with volumetric strains in the mainshock fault zone to be approximately 3 km, with secondary faulting (i.e., large aftershocks on distinct faults) extending to distances greater than 5 km from the mainshock fault.

3.5 Largest Aftershock of the WPAS

As of 7th August 2024, the largest recorded aftershock in the WPAS was a Ml 4.7 earthquake in June 2023. The largest aftershock, with a magnitude 1.1 lower than the mainshock, occurred approximately 1.7 years (646 days) after the mainshock. According to Modified Bath's Law (Shcherbakov & Turcotte, 2004), the expected largest aftershock magnitude for a Ml 5.8 mainshock is a Ml 4.7, which is consistent with the WPAS. Typically, the median time interval between the mainshock and the largest aftershock is 3 days, with the largest aftershock more likely to occur earlier in the sequence (Tahir et al., 2012). Ebel (2009) calculated a 40% probability that the largest aftershock in SCRs would occur within 5 days of the mainshock, a 70% probability within 60 days, and a 30% probability greater than 60 days. The 647-day interval between the mainshock and the largest aftershock in the WPAS represents a delayed occurrence compared to other SCR aftershock sequences. Additionally, the distance of the largest observed aftershock at Woods Point is approximately 4.6 to 5.1 km from the mainshock rupture plane. The presence of the largest aftershock occurring greater than 5km from the mainshock is consistent with other global aftershock sequences, including the Mw 7.3 1992 Landers earthquake, USA, where the largest aftershock (Mw 6.2) occurred approximately 30 km west of the mainshock (Hauksson et al., 1993)., and the Mw 7.1 2010 Darfield earthquake, NZ, where the largest aftershock (Mw 6.1) occurred approximately 40 km east of the mainshock (Li et al., 2014).

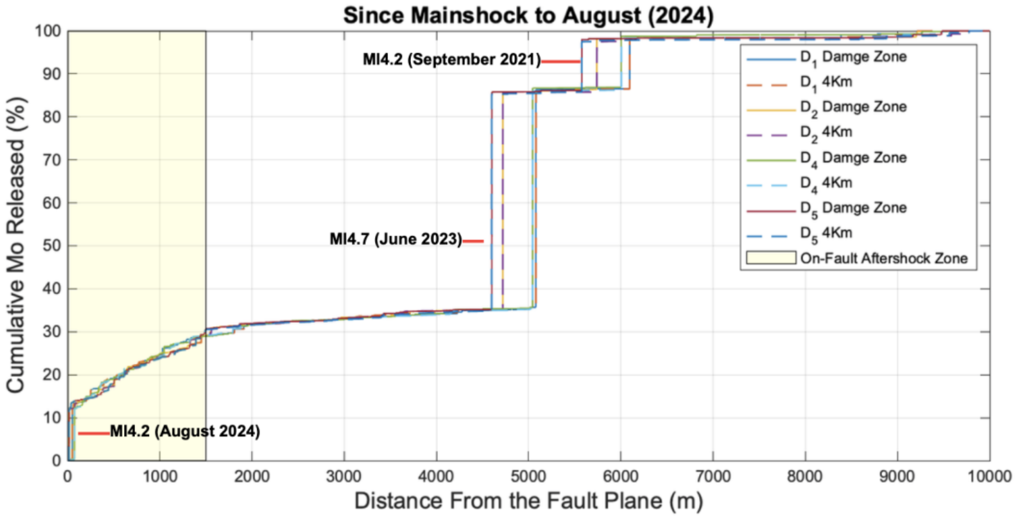

Figure 5. The relationship between the energy released by observed aftershocks and their distance from the respective fault planes. This figure uses the catalogue of aftershocks observed from the mainshock until 7th August 2024 within a 20 km radius from the mainshock's hypocenter. The spatial distribution of energy was analysed based on the rupture plane location determined in this study. The maximum curvature zone for the Woods Point earthquake is approximately 1.03 km to 1.45 km from the fault plane, rounded to a 1.5 km cutoff zone, highlighted in yellow. D1, D2, D4, and D5 represent the subdatasets. For more information, please refer to Appendix 2, please visit https://github.com/Yunqi12/Data-Description-Methodology.

4 Conclusions

1. b-value Estimation: The WPAS shows a b-value between 0.76 and 1.07, consistent with the synthetic background seismicity (Leonard, 2008) at 0.9 and the regional b-value (Allen et al., 2018) at 1.08. However, our estimated b-value for the pre-mainshock background seismicity is lower, ranging from 0.58 to 0.73. This may be less accurate due to the small sample size (93 to 197 events), influenced by sampling errors arising from the limited time and spatial windows, as well as the chosen Mc (ranging between 2.03 and 2.3). Additionally, the magnitude type used in the analysis impacts the b-value calculation due to the non-linear conversion between Ml and Mw.
2. Modelled Duration of Aftershock Sequence: Estimates of WPAS duration range from 7.5 to 40.4 years. As of 7 August 2024 (approximately 3 years after the mainshock), we determined that the WPAS could continue for several decades before the seismicity rates align with pre-mainshock background levels. The spatial distribution of WPAS does not yet conform to the synthetic background seismicity distribution, and monthly energy release is still above pre-mainshock levels.
3. Rupture Plane Fitting: The fault plane identified from the WPAS, aligns with published focal mechanisms and waveform analyses, showing a strike of 352.81° ± 3.2° and a near-vertical dip of 85.50°E ± 2.97°. The fault plane's dimensions range from 4.8 to 6.6 km in length and 6.77 to 9.31 km in width, with rupture depths varying from 7.63 to 17.82 km.
4. On-fault Aftershock Zone: We delineate the on-fault aftershock zone to extend 1.5 km on each side of the fault plane. We find this zone accounts for 29.4% of the total energy released from near-source seismicity, including the Ml 4.2 earthquake in August 2024. The two other largest aftershocks, Ml 4.7 in June 2023 and Ml 4.2 in September 2021, are considered off-fault aftershocks.
5. Delay of Largest Aftershock: The expected largest aftershock, around Ml 4.7 (using Modified Bath's law), matches the observed largest aftershock in June 2023. However, the 1.7-year interval between the mainshock and the largest aftershock is significantly longer than in other SCR aftershock sequences, as statistical analysis shows that in 70% of cases, the largest aftershocks in SCRs occur within 60 days (Ebel, 2009).

5 Acknowledgements

We thank Trevor Allen, Dan Sandiford, Yuxiang (Gideon) Tang and Dee Ninis for scientific discussions relating to this work. This research was funded by AuScope https://www.auscope.org.au/.

We also thank the National Emergency Management Authority for funding this research under the Disaster Ready Scheme Project DR40204.

6 References

Aki, K. (1965). Maximum likelihood estimate of b in the formula log10N = a - bm and its confidence limits. *Bulletin of Earthquake Research, 43*, 237-239.

Allen, T. I., Griffin, J., Ghasemi, H., Leonard, M., & Clark, D. (2018). *The 2018 national seismic hazard assessment for Australia: Model overview*. Geoscience Australia.

Attanayake, J., Jones, A., Gibson, G., & Sandiford, M. (2023). Pre-commercial baseline passive seismic monitoring around CarbonNet's Pelican Site in the offshore Gippsland Basin, Victoria—The first five years. *International Journal of Greenhouse Gas Control*, *128*, 103962.

Cao, A., & Gao, S. S. (2002). Temporal variation of seismic b-values beneath northeastern Japan island arc. *Geophysical Research Letters, 29*(9), 48-1-48-3.

Ebel, J. E. (2009). Analysis of aftershock and foreshock activity in stable continental regions: Implications for aftershock forecasting and the hazard of strong earthquakes. *Seismological Research Letters*, *80*(6), 1062-1068.

Ebel, J. E., Bonjer, K. P., & Oncescu, M. C. (2000). Paleoseismicity: Seismicity evidence for past large earthquakes. *Seismological Research Letters*, *71*(2), 283-294.

Efron, B., & Tibshirani, R. J. (1994). *An introduction to the bootstrap*. Chapman and Hall/CRC.

Freed, A. M. (2005). Earthquake triggering by static, dynamic, and postseismic stress transfer. *Annual Review of Earth and Planetary Sciences, 33*(1), 335-367.

Godano, C., Lippiello, E., & de Arcangelis, L. (2014). Variability of the b value in the Gutenberg–Richter distribution. *Geophysical Journal International*, *199*(3), 1765-1771.

Hauksson, E., Jones, L. M., Hutton, K., & Eberhart-Phillips, D. (1993). The 1992 Landers earthquake sequence: Seismological observations. *Journal of Geophysical Research: Solid Earth*, *98*(B11), 19835-19858.

Hearn, E. H., Bürgmann, R., & Reilinger, R. E. (2002). Dynamics of Izmit earthquake postseismic deformation and loading of the Duzce earthquake hypocenter. *Bulletin of the Seismological Society of America, 92*(1), 172-193.

Helmstetter, A., & Sornette, D. (2003). Importance of direct and indirect triggered seismicity in the ETAS model of seismicity. *Geophysical Research Letters*, *30*(11).

Holschneider, M., Narteau, C., Shebalin, P., Peng, Z., & Schorlemmer, D. (2012). Bayesian analysis of the modified Omori law. *Journal of Geophysical Research: Solid Earth, 117*(B6).

Jordan, T.H., Chen, Y.T., Gasparini, P., Madariaga, R., Main, I., Marzocchi, W., Papadopoulos, G., Sobolev, G., Yamaoka, K. & Zschau, J. (2011). Operational earthquake forecasting: State of knowledge and guidelines for utilization. *Annals of Geophysic*s, 54(4), pp.315-391.

Leonard, M. (2008). One hundred years of earthquake recording in Australia. *Bulletin of the Seismological Society of America, 98*(3), 1458-1470.

Li, Q., Liu, M., & Stein, S. (2009). Spatiotemporal complexity of continental intraplate seismicity: Insights from geodynamic modeling and implications for seismic hazard estimation. *Bulletin of the Seismological Society of America*, *99*(1), 52-60.

Li, Y. G., De Pascale, G. P., Quigley, M. C., & Gravley, D. M. (2014). Fault damage zones of the M7. 1 Darfield and M6. 3 Christchurch earthquakes characterized by fault-zone trapped waves. *Tectonophysics*, *618*, 79-101.

Liu, M., & Stein, S. (2016). Mid-continental earthquakes: Spatiotemporal occurrences, causes, and hazards. *Earth-Science Reviews, 162*, 364-386.

Liu, Y. (2022). *Seishimi*. GitHub. https://github.com/yuankailiu/Seishimi

Lockner, D. A., Morrow, C., Moore, D., & Hickman, S. (2011). Low strength of deep San Andreas fault gouge from SAFOD core. *Nature*, *472*(7341), 82-85.

Mignan, A., & Woessner, J. (2012). Estimating the magnitude of completeness for earthquake catalogues. *Community Online Resource for Statistical Seismicity Analysis*. https://doi.org/10.5078/corssa-00180805. Available at http://www.corssa.org

Mousavi, S., Hejrani, B., Miller, M. S., & Salmon, M. (2023). Hypocenter, fault plane, and rupture characterization of Australian earthquakes: Application to the September 2021 Mw 5.9 Woods Point earthquake. *Seismological Society of America, 94*(4), 1761-1774.

Nava, F. A., Márquez-Ramírez, V. H., Zúñiga, F. R., Ávila-Barrientos, L., & Quinteros, C. B. (2017). Gutenberg-Richter b-value maximum likelihood estimation and sample size. *Journal of Seismology*, *21*, 127-135.

Ninis, D., Borleis, E., Quigley, M., Peck, W., & Wilcox, J. (2021, November). The Mw 5.9 Woods Point earthquake and aftershock sequence. In *Australian Earthquake Engineering Society 2021 Virtual Conference* (pp. 25-26).

Ogata, Y. (1983). Estimation of the parameters in the modified Omori formula for aftershock frequencies by the maximum likelihood procedure. *Journal of Physics of the Earth, 31*(2), 115-124.

Ozawa, S., & Ando, R. (2021). Mainshock and aftershock sequence simulation in geometrically complex fault zones. *Journal of Geophysical Research: Solid Earth*, *126*(2), e2020JB020865.

Parsons, T. (2002). Global Omori law decay of triggered earthquakes: Large aftershocks outside the classical aftershock zone. *Journal of Geophysical Research: Solid Earth*, *107*(B9), ESE-9.

Peng, Z., Ben-Zion, Y., Michael, A. J., & Zhu, L. (2003). Quantitative analysis of seismic fault zone waves in the rupture zone of the 1992 Landers, California, earthquake: evidence for a shallow trapping structure. *Geophysical Journal International*, *155*(3), 1021-1041.

Perrin, C., Waldhauser, F., & Scholz, C. H. (2021). The shear deformation zone and the smoothing of faults with displacement. *Journal of Geophysical Research: Solid Earth*, *126*(5), e2020JB020447. https://doi.org/10.1029/2020JB020447

Quigley, M. C., Hughes, M. W., Bradley, B. A., van Ballegooy, S., Reid, C., Morgenroth, J., Horton, T., Duffy, B., & Pettinga, J. R. (2016). The 2010–2011 Canterbury earthquake sequence: Environmental effects, seismic triggering thresholds and geologic legacy. *Tectonophysics*, 672, 228-274.

Quigley, M., Pascale, A., Clark, D., & Allen, T. (2021). Wednesday 22 September 2021 Mw 5.9 Woods Point earthquake – Information Sheet. Accessed at: https://learningfromearthquakes.org/2021-09-22-australia/images/2021_09_22-australia/pdfs/REPORT_EQ_27_SEPT_2021_short.TA.pdf

Shcherbakov, R., & Turcotte, D. L. (2004). A modified form of Bath's law. *Bulletin of the Seismological Society of America, 94*(5), 1968-1975.

Shcherbakov, R., Nguyen, M., & Quigley, M. (2012). Statistical analysis of the 2010 MW 7.1 Darfield Earthquake aftershock sequence. *New Zealand Journal of Geology and Geophysics*, *55*(3), 305-311.

Shi, Y., & Bolt, B. A. (1982). The standard error of the magnitude-frequency b value. *Bulletin of the Seismological Society of America, 72*(5), 1677-1687.

Stein, S., & Liu, M. (2009). Long aftershock sequences within continents and implications for earthquake hazard assessment. *Nature, 462*(7269), 87-89. https://doi.org/10.1038/nature08502

Sullivan, B., & Peng, Z. (2011). *Basic statistical seismology tutorial*. http://geophysics.eas.gatech.edu/people/bsullivan/tutorial/StatisticalSeismology.htm

Tahir, M., Grasso, J. R., & Amorese, D. (2012). The largest aftershock: How strong, how far away, how delayed?. *Geophysical Research Letters*, *39*(4).

Toda, S., & Stein, R. S. (2018). Why aftershock duration matters for probabilistic seismic hazard assessment. Bulletin of the Seismological Society of America, 108(3A), 1414-1426.

Utsu, T. (1965). A method for determining the value of b in a formula log n= a-bM showing the magnitude frequency relation for earthquakes. *Geophys. Bull. Hokkaido Univ.*, *13*, 99-103.

Utsu, T., Y. Ogata, & R. Matsu'ura (1995), The centenary of the Omori formula for a decay law of aftershock activity, *J. Phys. Earth*, **43**(1), 1–33.

Wiemer, S., & Wyss, M. (2000). Minimum magnitude of complete reporting in earthquake catalogues: examples from Alaska, the Western United States, and Japan. *Bulletin of the Seismological Society of America, 90*(4), 859–869.

Woessner, J., & Wiemer, S. (2005). Assessing the quality of earthquake catalogues: Estimating the magnitude of completeness and its uncertainty. *Bulletin of the Seismological Society of America, 95*(2), 684-698.

Wyss, M., Hasegawa, A., Wiemer, S., & Umino, N. (1999). Quantitative mapping of precursory seismic quiescence before the 1989, M 7.1 off-Sanriku earthquake, Japan. *Annals of Geophysics, 42*(5).

Yukutake, Y., & Iio, Y. (2017). Why do aftershocks occur? Relationship between mainshock rupture and aftershock sequence based on highly resolved hypocenter and focal mechanism distributions. *Earth, Planets and Space*, *69*, 1-15.